Nuclear Medicine and Biology 43 (2016) 642–649

Contents lists available at ScienceDirect

Nuclear Medicine and Biology

journal homepage: www.elsevier.com/locate/nucmedbio

Synthesis, in vitro and in vivo small-animal SPECT evaluation of novel technetium labeled bile acid analogues to study (altered) hepatic transporter function

Sara Neyt [a,*], Maarten Vliegen [b], Bjorn Verreet [b], Stef De Lombaerde [a], Kim Braeckman [c], Christian Vanhove [c], Maarten Thomas Huisman [b], Caroline Dumolyn [a], Ken Kersemans [a], Fabian Hulpia [d], Serge Van Calenbergh [d], Geert Mannens [b], Filip De Vos [a]

[a] Laboratory of Radiopharmacy, Ottergemsesteenweg 460, Ghent University, Ghent, Belgium
[b] Preclinical Development & Safety, Janssen Pharmaceutical Companies of Johnson & Johnson, Beerse, Belgium
[c] iMinds Medical IT-IBITech-MEDISIP-INFINITY, Ghent University, Ghent, Belgium
[d] Laboratory for Medicinal Chemistry, Ottergemsesteenweg 460, Ghent University, Ghent, Belgium

ARTICLE INFO

Article history:
Received 23 February 2016
Received in revised form 19 June 2016
Accepted 4 July 2016

Keywords:
Bile acid analogues
Technetium
Drug induced cholestasis
Small-animal SPECT
Hepatobiliary imaging

ABSTRACT

Introduction: Hepatobiliary transport mechanisms are crucial for the excretion of substrate toxic compounds. Drugs can inhibit these transporters, which can lead to drug–drug interactions causing toxicity. Therefore, it is important to assess this early during the development of new drug candidates. The aim of the current study is the (radio)synthesis, in vitro and in vivo evaluation of a technetium labeled chenodeoxycholic and cholic acid analogue: [^{99m}Tc]-DTPA-CDCA and [^{99m}]Tc-DTPA-CA, respectively, as biomarker for disturbed transporter functionality.
Methods: [99mTc]-DTPA-CDCA([**^{99m}Tc]-3a**) and [99mTc]-DTPA-CA ([**^{99m}Tc]-3b**) were synthesized and evaluated in vitro and in vivo. Uptake of both tracers was investigated in NTCP, OCT1, OATP1B1, OATP1B3 transfected cell lines. K_m and V_{max} values were determined and compared to [^{99m}Tc]-mebrofenin ([^{99m}Tc]-MEB). Efflux was investigated by means of CTRL, MRP2 and BSEP transfected inside-out vesicles. Metabolite analysis was performed using pooled human liver S9. Wild type (n = 3) and rifampicin treated (n = 3) mice were intravenously injected with 37 MBq of tracer. After dynamic small-animal SPECT and short CT acquisitions, time–activity curves of heart, liver, gallbladder and intestines were obtained.
Results: We demonstrated that OATP1B1 and OATP1B3 are the involved uptake transporters of both compounds. Both tracers show a higher affinity compared to [^{99m}Tc]-MEB, but are in a similar range as endogenous bile acids for OATP1B1 and OATP1B3. **[^{99m}Tc]-3a** shows higher affinities compared to **[^{99m}Tc]-3b**. V_{max} values were lower compared to [^{99m}Tc]-MEB, but in the same range as endogenous bile acids. MRP2 was identified as efflux transporter. Less than 7% of both radiotracers was metabolized in the liver. In vitro results were confirmed by in vivo results. Uptake in the liver and efflux to gallbladder + intestines and urinary bladder of both tracers was observed. Transport was inhibited by rifampicin.
Conclusion: The involved transporters were identified; both tracers are taken up in the hepatocytes by OATP1B1 andOATP1B3 with K_m and V_{max} values in the same range as endogenous bile acids and are secreted into bile canaliculi via MRP2. Dynamic small-animal SPECT imaging can be a useful noninvasive method of visualizing and quantifying hepatobiliary transporter functionality and disturbances thereof in vivo, which could predict drug pharmacokinetics.

1. Introduction

Bile acids play an essential role in the absorption of lipids, cholesterol and lipid-soluble vitamins in the intestinal lumen. They also affect intestinal and colonic epithelial function and integrity by triggering various signaling pathways [1,2]. The total bile acid pool in the human body is approximately 8 g. The majority of the bile acids undergoes efficient enterohepatic cycling, whereas 5% of the bile acids enter the colon and are excreted from the body. Driven by various nuclear hormone receptors, the homeostasis of bile acids is strictly regulated by a complex interplay of various mechanisms, consisting of uptake and efflux transporters at the liver and intestines and various CYP enzymes involved in the synthesis of bile acids from cholesterol. For example, in the liver sinusoids, the bile acids are taken up into the hepatocytes and secreted into the bile ducts, by active transport mechanisms [3]. Clinically relevant hepatic transport systems include the organic anion transport pumps (OATPs),

* Corresponding author at: Laboratory of Radiopharmacy, Ottergemsesteenweg 460, 9000 Gent, Belgium. Tel.: +32 9 264 80 45; fax: +32 9 264 80 71.
E-mail address: sara.neyt@ugent.be (S. Neyt).

http://dx.doi.org/10.1016/j.nucmedbio.2016.07.001
0969-8051/

sodium taurocholate cotransporting protein (NTCP), multidrug resistance protein 2 (MRP2) and bile salt export pump (BSEP).

Additionally, these hepatobiliary transport mechanisms are crucial for the overall excretion process of substrate toxic compounds, such as drugs, xenobiotics and toxins. This essential function makes the liver vulnerable to drug toxicity, since numerous drugs are substrates or inhibitors of hepatic transporters and hence, unexpected and unwanted interactions are frequently observed [4,5]. The interactions of drugs with these transporters can lead to toxic concentrations of bile acids or substrate drugs in blood or liver [6]. Since the inhibition of OATPs and MRP2 in itself possesses a moderate risk, it can increase the concentration of substrate drugs to elevated levels (e.g., statins), causing drug–drug interactions and toxicity [5]. Inhibition of NTCP or BSEP can lead to increased circulating bile salt levels or bile salt retention within the liver, which may lead to cholestasis, potentially resulting eventual in liver failure [1,7].

Therefore, it is important to assess the inhibition of hepatic transporters early during the development of new drug candidates. We previously reported that dynamic small-animal SPECT scanning of technetium labeled mebrofenin ([^{99m}Tc]-MEB) can be a suitable method to visualize and quantify disturbed hepatobiliary transport in a non-invasive manner [8]. However, MEB has no chemical similarities with endogenous bile acids. To assess non-invasively the effect of inhibition of hepatobiliary transporters on endogenous bile acids, there is a need for labeled bile acid analogues.

Previously, gadolinium (Gd)(III) [9], fluorescent [10,17], [^{18}F] [11] and [^{11}C] [12] labeled bile acid analogues were synthetized. Typically, these tracers have some shortcomings: Gd(III) labeled contrast agents do not allow for dynamic imaging and larger amounts have to be administered. The fluorescently labeled bile acid analogues have a lower tissue depth, the radioactive tracers labeled with ^{18}F and ^{11}C are difficult to synthetize (e.g., need for cyclotron) and ^{11}C tracers have a short half-life.

The aim of the current study is the (radio)synthesis of a technetium labeled chenodeoxycholic and cholic acid analogue (technetium labeled diethylene triamine pentaacetic acid chenodeoxycholic acid, [^{99m}Tc]-DTPA-CDCA and technetium labeled diethylene triamine pentaacetic acid chenodeoxycholic acid, [^{99m}]Tc-DTPA-CA, respectively). Technetium was used as radioisotope since it is easily produced (it can be eluted from a generator), its suitable half-life (6 h) and its limitless depth of penetration. Additionally, in vitro assays have been performed to identify the involved uptake and efflux transporters. Lastly, in vivo SPECT evaluation of normal and disturbed hepatobiliary transport has been performed to illustrate the ability of these agents to visualize and quantify (altered) hepatobiliary transport in vivo.

2. Materials and methods

2.1. General procedures and materials

Unless stated otherwise, all chemical reagents were obtained from commercial sources and used without further purification. [^{99m}Tc]O_4^- was eluted from a sterile [^{99m}Tc]-generator (Drytec; GE Healthcare). Exact mass measurements were performed on a Waters LCT Premier XETM Time of Flight (ToF) mass spectrometer equipped with a standard electrospray (ESI) and modular Lockspray TM interface. Samples were infused in a acetonitrile (MeCN)/water (1:1) + 0.1% formic acid mixture at 100 μL/min. Where reversed phase flash purification was performed, Reveleris C18 RP 12 g cartridges were used on a Reveleris X2 device (Grace) with a flow rate of 20 mL/min and a water:acetonitrile gradient (from 10 to 95% acetonitrile in 20 min; with 0.1% formic acid added to the solvents). Radiochemical yield/purity was determined by means of RP-HPLC (Econosphere C18 10 μm, length 250 mm, ID 10.0 mm (Grace)) with radiodetection (Ludlum Measurements Inc., Model 2200). A 20 min gradient was used at a flow rate of 6 mL/min (from 10 to 95% acetonitrile in 20 min; 0.1% formic acid). Radioactivity in cell lysates was acquired on an automatic gamma counter (COBRA, PerkinElmer). Chinese hamster ovary (CHO) cells, CHO-OCT, human embryonic kidney (HEK), and HEK293-OATP1B3 cells were purchased from Solvo Biotechnologies (Hungary); CHO-NTCP and HEK293-OATP1B1 cells were a kind gift from the same company. HEK293-MRP2, HEK293-BSEP and HEK293-CTRL vesicles were purchased from PharmTox (The Netherlands). Whole-body small-animal SPECT/CT acquisitions were acquired on a USPECTII/CT device (MILabs, the Netherlands).

2.2. Animal models

FVB mice (female; age: 5 weeks; weight: 20–25 g) were purchased from Janvier, and were housed and handled according to guidelines approved by the European Ethics Committee and acclimatized for at least 1 week before the experiments. All animals were kept under environmentally controlled conditions (12-h normal light/dark cycles, 20 °C–24 °C, and 40–70% relative humidity) with food and water ad libitum. The study protocol was approved by the Animal Experimental Ethical Committee of Ghent University (ECD12/62).

2.3. Chemistry

A summary of the (radio)synthesis is displayed in Fig. 1.

1. Synthesis of methyl (*R*)-4-((3*R*,5*S*,7*R*,8*R*,9*S*,10*S*,13*R*,14*S*,17*R*)-3,7-dihydroxy-10,13-dimethylhexadecahydro-1*H*-cyclopenta[a]phenanthren-17-yl)pentanoate (**1a**) and methyl (*R*)-4-((3*R*,5*S*,7*R*,8*R*,9*S*,10*S*,12*S*,13*R*,14*S*,17*R*)-3,7,12-trihydroxy-10,13-dimethylhexadecahydro-1*H*-cyclopenta[a]phenanthren-17-yl)pentanoate (**1b**)

Chenodeoxycholic and cholic acid (1 g, 2.55 and 2.45 mmol respectively) were dissolved in MeOH (5 mL). 2,2-dimethoxypropane (2.5 mL) and 0.15 mL 12 M hydrochloric acid were added. The resulting mixture was stirred at RT overnight and subsequently evaporated under reduced pressure [10]. Next, the residue was dissolved in EtOAc, washed with saturated $NaHCO_3$, brine, dried over $MgSO_4$, filtered and evaporated under reduced pressure till dryness to obtain **1a** and **1b** (91% and 83% yield, respectively), which were used in the next step without further purification. HRMS (ESI) calculated for **1a** [$C_{25}H_{42}O_4$] $[M + H]^+$: 407.3161, found: 407.3159; $[2\ M + H]^+$: 813.6249, found: 813.6251. MRMS (ESI) for **1b** [$C_{25}H_{42}O_5$] $[M + H]^+$: 423.3110, found: 423.3118; $[2\ M + H]^+$: 845,6137, found: 845,6198.

2. Synthesis of (*R*)-*N*-(2-aminoethyl)-4-((3*R*,5*S*,7*R*,8*R*,9*S*,10*S*,13*R*,14*S*,17*R*)-3,7 dihydroxy-10,13-dimethylhexadecahydro-1*H*-cyclopenta[a]phenanthren-17-yl)pentanamide (**2a**) and (*R*)-*N*-(2-aminoethyl)-4-((3*R*,5*S*,7*R*,8*R*,9*S*, 10*S*,12*S*,13*R*,14*S*,17*R*)-3,7,12-trihydroxy-10,13-dimethylhexadecahydro-1*H*-cyclopenta[a]phenanthren-17-yl)pentanamide (**2b**)

1a and **1b** (300 mg, 0.738 mmol and 0.710 mmol respectively) were dissolved in 10 mL MeOH and an excess of ethylenediamine (0.45 mL, 6.711 mmol) was added [13]. The reaction mixtures were stirred overnight at 50 °C. The solvents were evaporated under reduced pressure and the crude products were purified by column chromatography (20% (NH_3 7 M in MeOH) in DCM (*v*/*v*)) to give **2a** and **2b**. Compounds containing fractions were pooled and evaporated under reduced pressure. The resulting residue was stirred in di-isopropylether overnight, after which the materials were filtered and dried in vacuo to obtain **2a** and **2b** in 98% and 98% yield, respectively). MRMS (ESI) for **2a** [$C_{26}H_{46}N_2O_4$] $[M + H]^+$: 435.3581, found: 435.3585. MRMS (ESI) for **2b** [$C_{26}H_{46}N_2O_3$] $[M + H]^+$: 451.3531, found: 451.3488.

3. Synthesis of (*R*)-3,6,9-tris(carboxymethyl)-19-((3*R*,5*S*,7*R*,8*R*,9*S*,10*S*,13*R*,14*S*,17*R*)-3,7-dihydroxy-10,13-dimethylhexadecahydro-1*H*-cyclopenta[a]phenanthren-17-yl)-11,16-dioxo-3,6,9,12,15-pentaazaicosanoic acid (**3a**)and (*R*)-3,6,9-tris(carboxymethyl)-11,16-dioxo-19-((3*R*,5*S*,7*R*,8*R*,9*S*,10*S*,12*S*,13*R*,14*S*,17*R*)-3,7,12-trihydroxy-10,13-

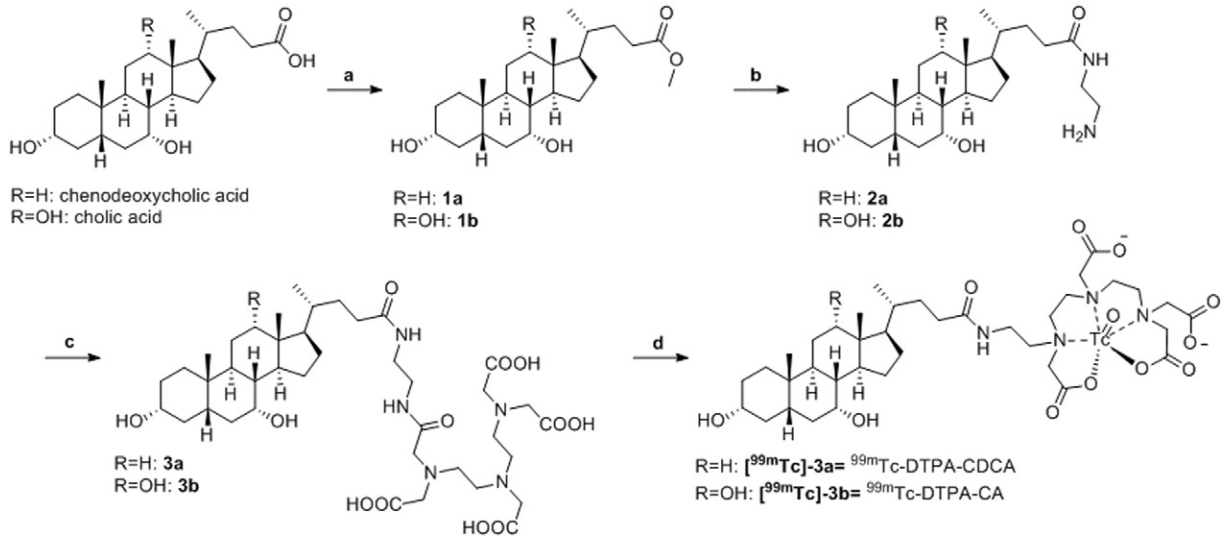

Fig. 1. Overview of the (radio)synthesis of the technetium labeled chenodeoxycholic acid analogue, [^{99m}Tc]-DTPA-CDCA ([**^{99m}Tc]-3a**) and cholic acid analogue, [^{99m}Tc]-DTPA-CA ([**^{99m}Tc]-3b**). Reagents and conditions: (a) dimethoxypropane, methanol, hydrochloric acid, 91% (**1a**), 83% (**1b**); (b) ethylenediamine, methanol, 98% (**2a**), 98% (**2b**); (c) dimethylformamide, triethylamine, DTPA(bis)anhydride, 26% (**3a**) and 16% (**3b**); (d) stannous chloride, pertechnetate ([[^{99m}Tc]]O_4^-), radiochemical purity >95%.

dimethylhexadecahydro-1*H*-cyclopenta[a]phenanthren-17-yl)-3,6,9,12,15-pentaazaicosanoic acid (**3b**)

2a and **2b** (97 mg, 0.450 mmol and 101 mg, 0.450 mmol respectively) were coupled to DTPA-bis-anhydride (120 mg, 0.338 mmol) [9]. Toward this end 5.5 μL (0.3 mmol) of water was added to a solution of DTPA-bis-anhydride and triethylamine (0.2 mL) in anhydrous DMF (10 mL). After 2 h of stirring at RT, **2a** or **2b** was added and stirring continued for 72 h. Then, the pH was adjusted to 7 with 6 M HCl. The solvent was evaporated under reduced pressure and the crude product was redissolved in 50:50 (*v*:*v*) MeCN:H2O. Subsequently, the products were purified by RP-flash chromatography (Reveleris X2; ELSD detection; column: reveleris C18, 12 g (Grace)) to give DTPA-CDCA (**3a**) and DTPA-CA (**3b**) in 26% and 16% yield, respectively. MRMS (ESI) for **3a** [$C_{40}H_{67}N_5O_{12}$] $[M + H]^+$: 810.4859, found: 810.4952. MRMS (ESI) for **3b** [$C_{40}H_{67}N_5O_{13}$] $[M + H]^+$: 826.4808, found: 826.4789. The total yield was 23% and 13% yield for **3a** and **3b**, respectively.

2.4. Radiosynthesis

[^{99m}Tc] incorporation was done by a direct labeling method [14] giving [^{99m}Tc]-DTPA-CDCA ([**^{99m}Tc]-3a**) and [^{99m}Tc]-DTPA-CA ([**^{99m}Tc]-3b**). To 2.25 ± 0.25 mg of compound dissolved in 50 μL saline in a shielded lead vial, 60 μL of 10^{-2} M $SnCl_2 \cdot 2H_2O$ solution (dissolved in N_2 purged 10% acetic acid) was added. Then, pH was adjusted to 6.5 with 0.2 M $NaHCO_3$, followed by addition of freshly eluted saline solution of sodium pertechnetate (185 MBq, 50 μL). Subsequently, the pH was again adjusted to 6.5 with 0.2 M $NaHCO_3$. The vial was allowed to incubate for 30 min at RT. Radiochemical purity was determined by means of RP-HPLC.

2.5. In vitro uptake assays

CHO-NTCP, CHO-OCT1, HEK293-OATP1B1 and HEK293-OATP1B3 cells were stably transfected with genes encoding human NTCP (*SLC10A1*), OCT1 (*SLC22A1*), OATP1B1 (*SLCO1B1*), and OATP1B3 (*SLCO1B3*) respectively. The cell lines were cultured in a humidified atmosphere at 37 °C in the presence of 5% CO_2. The culture medium of the CHO cells consisted of Dulbecco's modified Eagle's medium (DMEM)/F12, supplemented with 10% fetal calf serum, 2 mM L-glutamine, 0.3 mM L-proline, and antibiotics (Penicillin/Streptomycin; 50 U/mL; 50 μg/mL). The culture medium of the HEK293 cells consisted of DMEM glutamax; high glucose; pyruvate supplemented with 10% fetal calf serum, 5 mL MEM-non essential amino acid solution, and antibiotics (Penicillin/Streptomycin; 50 U/mL; 50 μg/mL).

For transport experiments, all CHO and HEK cells were seeded in 24-well plates (4.0×10^5 cells/well; n = 3/cell line) in 1 mL of the corresponding culture medium. After 18–24 h, medium was removed and cells were washed twice with washing buffer (1 mL sterile HBSS+/+ (HBSS with Ca^{2+} and Mg^{2+}), 10 mM HEPES, pH = 7.4, 37 °C). Incubation buffers (250 μL/well) were obtained by adding the radiolabeled compounds to the washing buffer. Final concentrations of the positive controls were 1 μM [^{3}H]-estradiol-17β-glucuronide (E17βG, for OATP1B1), 1 μM [^{3}H]-taurocholic acid (TCA, for NTCP) and 1 μM [^{14}C]-tetra-ethyl-ammonium (TEA, for OCT1). Concentrations of the test compounds ([^{99m}Tc]-DTPA-CDCA and [^{99m}Tc]-DTPA-CA) were 1, 2, 5, 10, 20, 50, 100, 250 μM (for all cell lines). Concentrations of [^{99m}Tc]MEB were 50, 100, 350, 1000, 2000, 5000 μM (for all cell lines). The plates were incubated at 37 °C and 5% CO_2 for 5, 10, 20, 30, 60, 90, 120, and 180 min. The incubation was stopped by placing the plates on ice and adding 1 mL of ice-cold HBSS+/+ with 1% BSA. Next, the cells were washed twice more with 2 mL HBSS+/+ and the supernatant was removed. The cells were lysed with 250 μL mammalian protein extraction reagent and the plates were shaken for 10 min at 400 rpm at RT. A 150 μL aliquot of this solution was used for gamma counting. Protein content was determined by means of a BCA kit (Thermo Scientific). The uptake in each cell line with and without inhibitor (100 μM rifampicin) was determined (pmol/mg protein). Additionally, the substrate concentrations were varied and the uptake rate (pmol/mg protein/min) was measured. Michaelis–Menten constants and associated maximum transport rates were calculated by means of GraphPad Prism (nonlinear regression).

2.6. In vitro vesicular efflux assay

To determine the involved efflux transporters, ATP-binding cassette transporter vesicles transfected with human MRP2 or BSEP were used (Pharmtox, the Netherlands). Membrane vesicles (7.5 μg of protein per well, n = 3/cell line) were incubated at 37 °C in a final volume of 30 μL. The buffer used was Tris (10 mM)/sucrose (250 mM) with or without 4 mM ATP, $MgCl_2$ (10 mM) and [^{99m}Tc]-DTPA-CDCA or [^{99m}Tc]-DTPA-CA (20 μM) and incubated for 15, 30, 60 or 90 min. The reaction was stopped by addition of 150 μL of ice-cold buffer and the well content was transferred to a glass fiber filter plate (Multiscreen HTS plates; Merck Millipore) and washed 3 times with buffer. Then,

100 μL 0.1 M NaOH was added and incubated at RT for 10 min to lyse the vesicles. An 80 μL aliquot of this solution was used for gamma counting.

2.7. Metabolite analysis

[^{99m}Tc]-DTPA-CDCA or [^{99m}Tc]-DTPA-CA (20 μM) was added to samples of pooled human liver S9 (Corning, USA) in potassium phosphate buffer (pH 7.4) with nicotinamide adenine dinucleotide phosphate (NADPH)-regenerating system solutions (Corning, USA). Samples without pooled human liver S9 and NADPH were used as controls and [^{99m}Tc]O4- or [99mTc]-DTPA was added to these control samples. All samples were incubated for 5, 10, 30 or 60 min at 37 °C. Acetonitrile was added and samples were placed on wet ice to stop the reaction. Samples were centrifuged at 13,000 ×*g* for 3 min. The supernatant was discarded, the extraction ratio was determined and the supernatant was analyzed for metabolites by using RP-HPLC (same protocol as the protocol used for quality control). Additionally, control samples were analyzed by RP-HPLC to determine the retention time of possible metabolites, [^{99m}Tc]O_4- or [^{99m}Tc]-DTPA.

2.8. Molecular imaging

Mice were imaged using a small-animal SPECT camera equipped with a cylindrical collimator containing 75 pinholes of 1 mm diameter (rat whole-body collimator; spatial resolution, 0.8 mm). All acquisitions were acquired in list mode.

After an overnight fast (minimum 6 h), mice (n = 6) were anesthetized with 1.5% isoflurane in medical O_2 to allow placement of intravenous polyethylene (PE10) tubing (Becton Dickinson, Belgium) in a lateral tail vein.

The mice were imaged while anesthetized, with their body temperature maintained during imaging using a heated bed.

Subsequently, in untreated mice (n = 3) a 120 min dynamic whole-body SPECT acquisition using 120 time frames of 1 min was initiated 5 s before the injection of 200 μL of [^{99m}Tc]-DTPA-CDCA or [^{99m}Tc]-DTPA-CA (37 MBq). Finally, a CT acquisition (50 kV tube voltage, 612 μA tube current, 5 min acquisition time) was performed for anatomical correlation.

Additionally, an in vivo inhibition experiment was performed. Mice (n = 3) were injected with rifampicin (100 mg/kg; IP) 60 min before tracer injection. Another dose of 25 mg/kg rifampicin was co-administered with the radiotracer (IV) and the same imaging protocol was performed.

All SPECT acquisitions were iteratively reconstructed using an ordered subsets expectation maximization algorithm (3 iterations; 16 subsets; 0.75 mm voxel size; decay correction), including from acquired list-mode data only those photons within an energy range of 140 keV ± 20%. Finally, regions of interest (ROIs) were manually drawn over the heart, liver, gallbladder + intestines and urinary bladder using PMOD software (PMOD technologies, Switzerland), with ROI volumes between 67 and 1578 mm^3. From the dynamic SPECT measurements, time–activity curves (TACs) were obtained.

To assess the linearity of the SPECT camera, 10 samples with predetermined amounts of $^{99m}TcO_4^-$ ranging from 0.37 MBq to 74 MBq and measured with a CRC-15R dose calibrator (Capintec, Ramsay, NJ) were scanned using the same dynamic acquisition protocol. The resulting calibration curve was used to quantify the amount of radioactivity. The total activity in each organ, expressed in MBq or MBq/mL (blood) (normalized to an injection of 37 MBq and a mouse weight of 20 g), was expressed as a function of time (in seconds).

2.9. Statistical analysis

Statistical analysis was performed using Prism, version 3.0 (GraphPad), and SPSS version 22, version 22, for Windows (Microsoft). For the in vitro uptake and efflux assays, uptake in function of time was determined. Additionally, Michaelis–Menten constants and associated maximum transport rates were calculated by means of GraphPad Prism (nonlinear regression). The time–activity curves were described by calculating the maximal tracer amount (C_{max}) in the liver and in the gallbladder and intestines, the time point at which tracer maximized (time to peak) in the liver, and the AUC in the blood, liver and gallbladder and intestines. AUCs were calculated using the trapezoidal method. Differences between 2 groups were tested for significance using the nonparametric Mann–Whitney test for 2 groups. All experiments were performed on 3 samples (unless stated otherwise); a *p* value of 0.05 or smaller was considered significant.

3. Results

3.1. Radiosynthesis

Radiochemical purities were higher than 95% within 30 min. In its final formulation or dissolved in the appropriate buffer for the in vitro experiment, the tracers showed no alterations in radiochemical purity for up to 4 h after the end of the synthesis.

3.2. In vitro uptake assays

The transfected cell lines are fully functional, which is confirmed by the uptake of positive controls. The uptake of [^{3}H]-TCA, [^{14}C]-TEA and [^{3}H]-E17-BG is 255-, 11-, 256- and 50-fold higher in CHO-NTCP, CHO-OCT1, HEK293-OATP1B1 and HEK293-OATP1B3, respectively compared to their parent/mock cell line.

Fig. 2 shows the in vitro uptake of 20 μM [^{99m}Tc]-DTPA-CDCA (**[^{99m}Tc]-3a**) and [^{99m}Tc]-DTPA-CA (**[^{99m}Tc]-3b**) after 60 min (A and C, respectively) and with or without rifampicin co-incubation (B, D, respectively). Without inhibitor, significantly higher uptake is observed for both tracers in HEK293-OATP1B1 and -OATP1B3 compared to their controls, HEK293-MOCK. After 60 min, the uptake of [^{99m}Tc]-DTPA-CDCA is 534.2 ± 6.0 and 316.8 ± 8.1 pmol/mg protein in OATP1B1 and OATP1B3 transfected cell lines, respectively. The uptake in the MOCK transfected cell lines was 82.2 ± 4.9 pmol/mg protein. The uptake of [^{99m}Tc]-DTPA-CA was 212 ± 7.6, 110.9 ± 2.1 and 50.8 ± 1.7 pmol/mg protein in OATP1B1, OATP1B3 and MOCK transfected cell lines, respectively. For both tracers, no significant higher uptake was observed in NTCP and OCT1 transfected cell lines.

After co-incubation with 100 μM rifampicin, a known OATP inhibitor, the uptake is significantly lower for both tracers in the OATP transfected cell lines. The uptake of [^{99m}Tc]-DTPA-CDCA after rifampicin administration amounts to 100.2 ± 13.9 and 87.9 ± 13.4 pmol/mg protein in OATP1B1 and OATP1B3 cell lines, respectively. The uptake of [^{99m}Tc]-DTPA-CA after rifampicin administration amounts to 72.4 ± 1.6 and 85.8 ± 1.9 pmol/mg protein in OATP1B1 and OATP1B3 cell lines, respectively.

Fig. 3 depicts uptake kinetics for [^{99m}Tc]-DTPA-CDCA (**[^{99m}Tc]-3a**, Fig. 3A); [^{99m}Tc]-DTPA-CA (**[^{99m}Tc]-3a**, Fig. 3B) and [^{99m}Tc]-MEB (Fig. 3C). The uptake was saturable with increasing concentrations of substrate for all three tracers and for both cell lines (OATP1B1 and OATP1B3 transfected cell lines). The Michaelis–Menten constants (K_m) with associated maximum transport rates (V_{max}) were calculated (Table 1). Both tracers show a higher affinity compared to [^{99m}Tc]-MEB. The lower K_m of [^{99m}Tc]-DTPA-CDCA indicates a higher affinity for both OATP1B1 and OATP1B3 compared to [^{99m}Tc]-DTPA-CA. The affinity for OATP1B1 is higher than the affinity for OATP1B3, for all the tracers. V_{max} values of [^{99m}Tc]-DTPA-CDCA and [^{99m}Tc]-DTPA-CA were lower compared to V_{max} value of MEB, indicating slower transport.

3.3. In vitro vesicular efflux assay

To determine the involved efflux transporters, ATP-binding cassette transporter vesicles transfected with human MRP2 or BSEP were used. The ATP-dependent [^{99m}Tc]-DTPA-CDCA and [^{99m}Tc]-DTPA-CA uptake

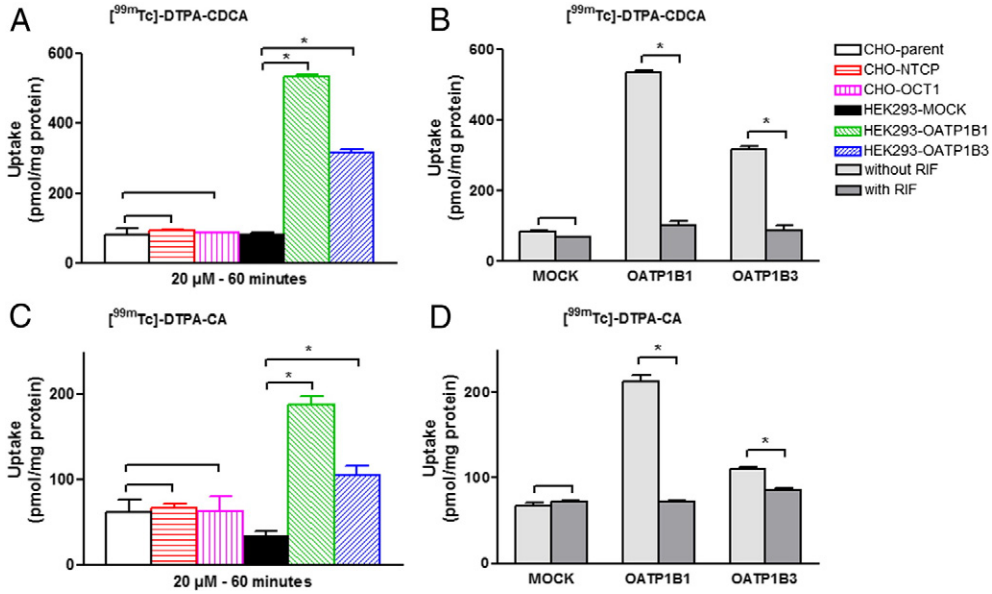

Fig. 2. In vitro uptake of 20 μM[^{99m}Tc]-DTPA-CDCA (**[^{99m}Tc]-3a**) (A) and [^{99m}Tc]-DTPA-CA (**[^{99m}Tc]-3b**) (C) after 60 min. Uptake of 20 μM[^{99m}Tc]-DTPA-CDCA (**[^{99m}Tc]-3a**) and [^{99m}Tc]-DTPA-CA (**[^{99m}Tc]-3b**) after 60 min with or without co-incubation with 100 μM rifampicin (B, D, respectively) (n = 3).

was determined in canalicular inside-out membrane vesicles by a rapid filtration method. A time dependent uptake of the tracers was observed in presence of ATP in MRP2 vesicles (Fig. 4). We observed a significant higher uptake in MRP2 vesicles in ATP+ conditions compared to ATP− conditions after 15, 30, 60 and 90 min for [^{99m}Tc]-DTPA-CDCA; and after 30, 60 and 90 min for [^{99m}Tc]-DTPA-CA ($p \leq 0.05$). There was no difference in uptake in ATP+ and ATP− conditions for control and BSEP vesicles at all time points.

3.4. Metabolite analysis

Table 2 shows the metabolic analysis of [^{99m}Tc]-DTPA-CDCA and [^{99m}Tc]-DTPA-CA in pooled human liver S9. Elution times of [^{99m}Tc]TcO_4^-, [^{99m}Tc]-DTPA, [^{99m}Tc]-DTPA-CDCA and [^{99m}Tc]-DTPA-CA are 2.25, 1.61, 5.30 and 4.98 min, respectively. At all time points, the percentage of the [^{99m}Tc]-DTPA-CDCA and [^{99m}Tc]-DTPA-CA did not go below 96 and 93%, respectively.

3.5. Molecular imaging

In vivo SPECT imaging of mice revealed uptake of both radiotracers in liver, gallbladder, intestines and urinary bladder. Fig. 5 shows static reconstructions of [^{99m}Tc]-DTPA-CDCA (Fig. 5A, B) and [^{99m}Tc]-DTPA-CA (Fig. 5C, D) during the first 10 min (early phase, Fig. 5A and C) and during the last 110 min (late phase, Fig. 5B and D) of the SPECT acquisitions. In the early phase, [^{99m}Tc]-DTPA-CDCA is taken up in the liver, gallbladder and urinary bladder. [^{99m}Tc]-DTPA-CA is taken up in liver and urinary bladder. In the late phase, the mean distribution of the tracers show mainly uptake in the intestines and urinary bladder.

Time–activity curves of [^{99m}Tc]-DTPA-CDCA and [^{99m}Tc]-DTPA-CA in WT and rifampicin treated mice are shown in Fig. 6 and the corresponding metrics are shown in Table 3.

[^{99m}Tc]-DTPA-CDCA (Fig. 6A) and [^{99m}Tc]-DTPA-CA (Fig. 6C) show uptake in the liver with a maximal uptake of respectively 13.83 ± 0.58 MBq and 9.50 ± 1.45 MBq at 12.67 ± 1.53 MBq and 12.00 ± 1.00 min, followed by a decrease to baseline levels, indicating secretion.

A secretion maximum to gallbladder and intestine of 23.00 ± 2.00 MBq and 17.67 ± 2.61 MBq for [^{99m}Tc]-DTPA-CDCA and [^{99m}Tc]-DTPA-CA, respectively, indicates secretion of the radiotracer to gallbladder and intestines. Additionally, in the urinary bladder, an accumulation of activity was observed with a maximal uptake of respectively 5.10 ± 0.71 and 13.00 ± 1.98 MBq (Fig. 6A, B, Table 3). After 4 h, the remaining radioactivity was located in the intestines and no activity was observed in the urinary bladder, since the urinary bladder was emptied.

Next, we investigated the effect of rifampicin administration on [^{99m}Tc]-DTPA-CDCA and [^{99m}Tc]-DTPA-CA transport. Rifampicin is both a substrate and an inhibitor of OATPs and MRP2, and therefore, it was selected as test agent. The time–activity curves of the rifampicin treated mice (100 mg/kg intraperitoneally, 25 mg/kg intravenously) are shown in Fig. 6B and D. Corresponding metrics are shown in Table 2. Compared to control mice, the maximum liver uptake was 2.6- and 2.8-fold lower in rifampicin treated mice compared to control mice ($p \leq 0.05$) for [^{99m}Tc]-DTPA-CDCA and [^{99m}Tc]-DTPA-CA, respectively. Additionally, the liver AUC was 1.5- and 3.1-fold lower in rifampicin treated mice for [^{99m}Tc]-DTPA-CDCA and [^{99m}Tc]-DTPA-CA, respectively.

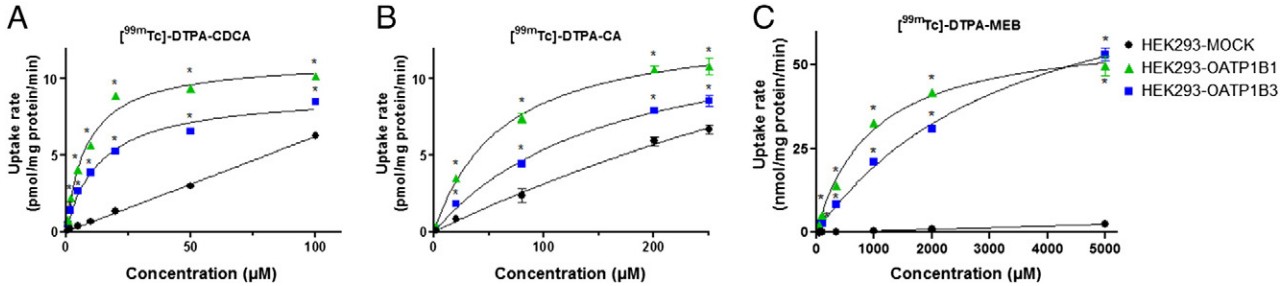

Fig. 3. In vitro uptake of [^{99m}Tc]-DTPA-CDCA (**[^{99m}Tc]-3a**, A), [^{99m}Tc]-DTPA-CA (**[^{99m}Tc]-3b**, B) and [^{99m}Tc]-MEB (C) (n = 3).

Table 1
Michaelis–Menten constants and associated maximum transport rates of [^{99m}Tc]-DTPA-CDCA ([**^{99m}Tc]-3a**) and [^{99m}Tc]-DTPA-CA ([**^{99m}Tc]-3b**) and [^{99m}Tc]-MEB determined by means of nonlinear regression.

		K_m (μM)	V_{max} (pmol/mg protein/min)
[^{99m}Tc]-DTPA-CDCA	HEK293-OATP1B1	8.45 ± 0.75	11.3 ± 0.29
	HEK293-OATP1B3	13.7 ± 1.24	9.10 ± 0.27
[^{99m}Tc]-DTPA-CA	HEK293-OATP1B1	61.7 ± 5.25	13.6 ± 0.36
	HEK293-OATP1B3	162 ± 16.9	14.1 ± 0.70
[^{99m}Tc]-MEB	HEK293-OATP1B1	958 ± 78.8	(60.5 ± 1.70) × 10^3
	HEK293-OATP1B3	3547 ± 294	(90.2 ± 3.97) × 10^3

Table 2
Metabolite analysis of [^{99m}Tc]-DTPA-CDCA and [^{99m}Tc]-DTPA-CA in pooled human liver S9.

	Retention time (min)	QC	5 min	10 min	30 min	60 min
[^{99m}Tc]-DTPA-CDCA	2.25	2%	3%	3%	4%	5%
	4.98	98%	97%	97%	96%	95%
[^{99m}Tc]-DTPA-CA	2.25	2%	4%	5%	5%	7%
	5.30	98%	96%	95%	95%	93%
[^{99m}Tc]-DTPA	1.61	100%	100%	100%	100%	100%
[^{99m}Tc]TcO_4^-	2.25	100%	100%	100%	100%	100%

Elution times of [^{99m}Tc]TcO_4^-, [^{99m}Tc]-DTPA, [^{99m}Tc]-DTPA-CDCA and [^{99m}Tc]-DTPA-CA are 2.25, 1.61, 4.98 and 5.30 min, respectively.

In rifampicin treated mice the AUC and the maximal tracer activity in the gallbladder and intestine for [^{99m}Tc]-DTPA-CDCA were 7.6 times lower compared to control animals. For [^{99m}Tc]-DTPA-CA, the maximal tracer activity in the gallbladder and intestine was 36 times lower and gallbladder/intestine AUC was 32 times lower, when rifampicin treated mice are compared to control animals. The mean blood AUC in RIF treated mice was 2.6-fold and 2.1-fold greater than in their control counterparts. There was no significant difference between urinary bladder C_{max} and AUC.

4. Discussion

Drug-induced liver injury is one of the leading causes for the withdrawal of approved drugs from the market, highlighting the importance of assessing this effect early on in drug research. One of the underlying causes of drug-induced liver injury is an altered functional activity of hepatic uptake or efflux transporters [5].

[^{99m}Tc]-MEB is an OATP1 and MRP2 substrate that is used in nuclear medicine to investigate the (dys)function of liver and gallbladder. We previously demonstrated the ability of non-invasively visualizing and quantifying disturbed hepatic transport by drugs or genetic defects by means of small-animal SPECT imaging of [^{99m}Tc]-MEB [8]. However, MEB is a lidocain analogue and has no similarities with endogenous bile acids. Therefore, in the current study, a procedure for the synthesis and radiolabeling of two bile acid analogues was developed, which resemble endogenous primary bile acids, for in vitro uptake and efflux experiment and in vivo small-animal SPECT studies. These compounds can possibly be used to investigate the disturbances of hepatobiliary transport mechanisms by drugs in vivo. DTPA-chenodeoxycholic acid (DTPA-CDCA, **3a**) and DTPA-cholic acid (DTPA-CA, **3b**) were synthetized from respectively chenodeoxycholic and cholic acid by esterification with methanol, exchange of the methylester with ethylenediamine and subsequent coupling with DTPA-bis-anhydride as chelating agent [9,10,13]. Finally, these bile acid analogues were successfully labeled by technetium incorporation.

In vitro evaluation of both compounds showed that the human uptake transporters OATP1B1 and OATP1B3 are clearly involved in the uptake of both tracers. For [^{99m}Tc]-DTPA-CDCA, K_m values of 8.45 ± 0.75 μM and 13.7 ± 1.24 μM were obtained for OATP1B1 and OATP1B3, respectively. For [^{99m}Tc]-DTPA-CA, these values were 61.7 ± 5.25 μM and 162 ± 16.9 μM, respectively. When these K_m values are compared to the K_m values of endogenous bile acids, similar values were observed (K_m OATP1B1 cholate: 11.4 ± 2.3 μM for OATP1B1 [15]; K_m Oatp1 taurocholic acid: 19.4 ± 3.3 μM, K_m taurodeoxycholic acid: 3.5 ± 0.25 μM [16]). Additionally, similar transport was observed of the previously reported fluorescent tracer cholyl-l-lysyl-fluorescein (CLF) [17,18]. The structures of [^{99m}Tc]-DTPA-(CD)CA are comparable to that of CLF, because all three structures are primary bile acids with modifications on the carboxyl moiety. K_m values of CLF were in the same range as [^{99m}Tc]-DTPA-(CD)CA. (K_m for OATP1B3 of CLF was 4.6 ± 2.7 μM; no K_m-value of OATP1B1 was reported). When the newly synthetized tracers were compared with the lidocain analogue [^{99m}Tc]-MEB, which is commonly used in nuclear medicine for hepatobiliary imaging, lower K_m values were observed (K_m values of MEB of 957 ± 78.8 μM and 3547 ± 294 μM; for OATP1B1 and OATP1B3, respectively). The contribution of the active components is thus larger for the bile acid analogues compared to MEB, resulting in a higher affinity (lower K_m).

V_{max} values of [^{99m}Tc]-DTPA-CDCA and [^{99m}Tc]-DTPA-CA were lower compared to that of MEB, indicating that the efficiency of the active transport is much lower for the bile acid analogues (Table 1). However, the transport rates which are observed for [^{99m}Tc]-DTPA-CDCA and [^{99m}Tc]-DTPA-CA are in the same range as the transport rates of endogenous chenodeoxycholic acid and cholic acid (V_{max} Oatp1 taurocholic acid = 62 ± 1.4 pmol/mg protein/min; V_{max} Oatp1 taurodeoxycholic acid = 199 ± 27 pmol/mg protein/min [16]). In conclusion, the synthesized bile acid analogues show more similarities to endogenous bile acid transport, in comparison with MEB.

Additionally, our data confirms previous studies that the side chain of bile salts is essential for NTCP transport. Baringhaus et al. [19] determined the pharmacophore of both NTCP and ASBT (ASBT is the ileal counterpart, NTCP and ASBT are homologous bile salt transporters) and found that the 3-OH group is not essential for transport by these transporters, in contrast to the acidic side chain. Our data are completely in line with this model. In contrast to [^{99m}Tc]-DTPA-(CD)CA, a fluorescent bile salt conjugate taurocholylchlorambucil, was found to be a substrate for human NTCP [20]. This compound is conjugated at the 3-OH position of the bile acid, whereas our compounds are conjugated at the side chain. This confirms that the 3-OH position is not essential for transport, whereas the side chain is. The less specific bile salt transporters,

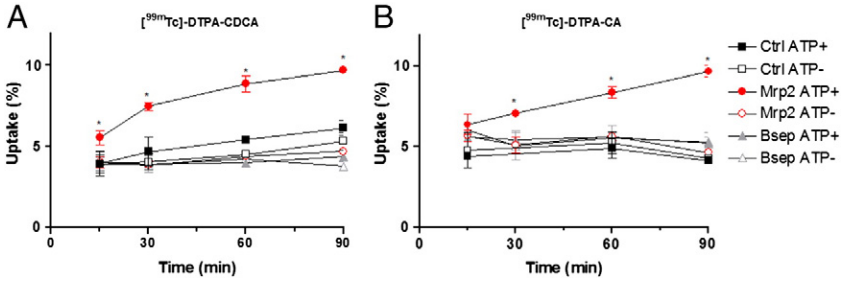

Fig. 4. In vitro vesicular efflux assay. Uptake of 20 μM [^{99m}Tc]-DTPA-CDCA ([**^{99m}Tc]-3a**, A) and [^{99m}Tc]-DTPA-CA ([**^{99m}Tc]-3b**, B) after 15, 30, 60 and 90 min.

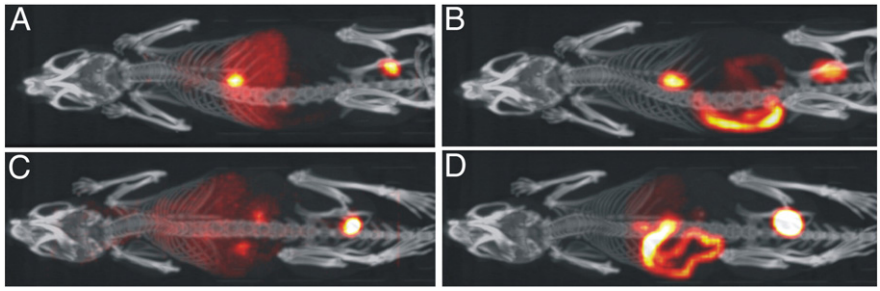

Fig. 5. Projection images of co-registered CT and small-animal SPECT images of 37 MBq [^{99m}Tc]-DTPA-CDCA ([**^{99m}Tc]-3a**) (A, B) and [^{99m}Tc]-DTPA-CA ([**^{99m}Tc]-3b**) (C, D) during the first 10 min (A, C) and during the last 110 min (B, D) of the dynamic SPECT acquisition (120 frames, 1 min/frame). Mice were anesthetized with 1.5% isoflurane in medical O_2.

OATP1B1 and OATP1B3, are more likely to be involved in uptake of [^{99m}Tc]-DTPA-(CD)CA into the hepatocyte, which is in line with the broad substrate specificity of these transporters [21]. After co-incubation with rifampicin, a known OATPs inhibitor, uptake of [^{99m}Tc]-DTPA-CDCA in OATP1B1 and OATP1B3 transfected cell lines was 5- and 4- fold reduced, respectively. Uptake of [^{99m}Tc]-DTPA-(CD)CA was 2 and 1.3-fold reduced, respectively. Consequently, this also confirms that these two transporters are involved in the uptake of [^{99m}Tc]-DTPA-CDCA and [^{99m}Tc]-DTPA-CA, since rifampicin is a known pan-OATP inhibitor [8].

Finally, a difference in in vitro uptake between the two analogues was observed, probably due to the presence or absence of the hydroxyl group at the C12 position. Our findings are in agreement with Hata et al. [16], who stated that the transport of trihydroxy bile acids was below that of dihydroxy bile acids. Indeed, we also reported that the transport of the trihydroxy analogue, [^{99m}Tc]-DTPA-CA is 2.5- and 3-fold lower, in respectively OATP1B1 and OATP1B3 transfected cell lines respectively, compared to the transport of the dihydroxy analogue [^{99m}Tc]-DTPA-CDCA. This difference in transport was also reflected in the in vivo results.

Vesicular efflux experiments identified MRP2 as the involved efflux transporter, and not BSEP. Uptake in MRP2 transfected inside-out vesicles at 60 min was respectively 2- and 1.5-fold higher in presence of ATP, compared to conditions without ATP. This is in accordance with the findings of Gerloff et al. [22], who demonstrated that unconjugated cholate is not transported by rat Bsep. This is also supported by the observation that in patients with a defect in bile acid conjugation practically no unconjugated bile acids are found in bile [23]. Additionally, de Waart et al. [17], stated that CLF is no BSEP substrate. There seems to be a negative correlation between BSEP substrates and molecular weight. MRP2, in contrast, can accommodate larger molecules than BSEP. Since the molecular weight of these bile acid analogues in this study was almost doubled due to DTPA coupling to the primary bile acid, efflux transport by MRP2 and not BSEP can be explained to the size of the analogues. Our findings are thus completely in line.

Metabolite analysis was performed using pooled human liver S9 and RP-HPLC [24]. A very small amount of radiotracer was metabolized in the liver to [^{99m}Tc]TcO_4^- (less than 7%). No modifications on the steroid nucleus of the bile acid analogues were observed.

Preclinical in vivo evaluation revealed that both compounds showed uptake in the liver and efflux to gallbladder and intestines. [^{99m}Tc]-DTPA-CDCA showed more uptake in the liver and efflux to gallbladder and intestines compared to [^{99m}Tc]-DTPA-CA that is cleared in a higher extent by the kidneys. This is in line with the findings of Hata et al. [16], who stated that dihydroxy bile acids show better transport compared to trihydroxy bile acids. Additionally, our in vitro data also support these in vivo findings: uptake of [^{99m}Tc]-DTPA-CA was lower compared to [^{99m}Tc]-DTPA-CDCA in transfected OATP1B1 and OATP1B3 cells. No enterohepatic recirculation was observed for both compounds. Asbt is the ileal counterpart (homologous bile salt transporters) of Ntcp [25], and consequently, these in vivo data, together with the finding that rifampicin can inhibit transport of both tracers, support the finding that Ntcp is not involved in transport of [^{99m}Tc]-DTPA-(CD)CA. Since

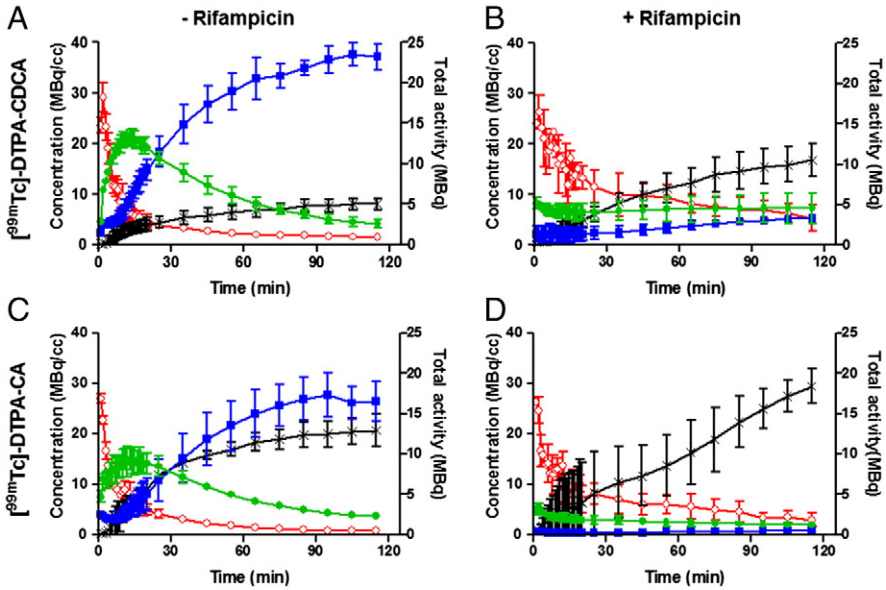

Fig. 6. Time–activity curves (TACs) of [^{99m}Tc]-DTPA-CDCA ([**^{99m}Tc]-3a**) (A, B) and [^{99m}Tc]-DTPA-CA ([**^{99m}Tc]-3b**) (C, D) in WT (n = 3) (A, C) and RIF treated (n = 3; 100 mg/kg IP, 60 min before imaging; 25 mg/kg IV, coinjected with tracer) (B, D) mice after intravenous injection of 37 MBq radiotracer and dynamic SPECT imaging (120 frames; 1 min/frame). ●: liver; ■: gallbladder + intestines; ×: urinary bladder; ○: blood. TAC_{heart} (blood) is expressed as MBq/mL (left y-axis); all other TACs are expressed as MBq (right y-axis). Data are mean ± SD. Mice were anesthetized with 1.5% isoflurane in medical O_2.

Table 3
Metrics of the time–activity curves of the heart (blood pool), liver, gallbladder/intestines and urinary bladder after injection of 37 MBq of tracer.

	[^{99m}Tc]-DTPA-CDCA	[^{99m}Tc]-DTPA-CDCA + RIF[a]	[^{99m}Tc]-DTPA-CA	[^{99m}Tc]-DTPA-CA + RIF[a]
Maximum liver uptake (MBq)	13.8 ± 0.58	5.2 ± 0.40	9.5 ± 1.45	3.37 ± 0.49
Liver time to peak (min)	12.7 ± 1.53	N/A	12.0 ± 1.00	N/A
Liver AUC (MBq × min)	755 ± 81.1	499 ± 157	582 ± 21.5	185 ± 52.0
Maximum secretion to gallbladder + intestines (MBq)	23.0 ± 2.00	3.30 ± 0.28	17.7 ± 2.61	0.48 ± 0.8
Gallbladder + intestines AUC (MBq × min)	1926 ± 178	253 ± 67.9	1250 ± 171	39.0 ± 15.6
Urinary bladder C_{max} (MBq)	5.10 ± 0.71	10.6 ± 2.05	13.0 ± 1.98	18.5 ± 2.19
Urinary bladder AUC (MBq × min)	425 ± 85	758 ± 182	1093 ± 80.6	1098 ± 397
Blood AUC (MBq/mL × min)	426 ± 125	1138 ± 262	353 ± 58.3	742 ± 217

n = 3 per group; mean (n = 3) ± SD. AUC = area under the curve. RIF = rifampicin.
[a] 100 mg/kg intraperitoneal 60 min before tracer injection; 25 mg/kg intravenous, coinjected with tracer.

there is no recirculation of these bile acids analogues, the radiation dose is reduced.

Our in vitro data also support the in vivo findings of the current study and a previous study in which we investigated the hepatobiliary transport of [^{99m}Tc]-MEB [8]. We observed lower V_{max} values for [^{99m}Tc]-DTPA-(CD)CA compared to MEB. In vivo, we also observed slower transport compared to [^{99m}Tc]-MEB. The time to peak in the liver was 2.5 min for [^{99m}Tc]-MEB, whereas the time to peak was 12.00 and 12.67 min for [^{99m}Tc]-DTPA-CDCA and [^{99m}Tc]-DTPA-CA, respectively.

Determination of the influence of newly synthetized drugs on liver transporters is important to detect possible pharmacological inhibition which can lead to hepatotoxicity. To assess the effect of pharmacological inhibition on transporter activity, rifampicin was administered as model drug, by both the intraperitoneal and the intravenous routes. This double administration led to impaired uptake of both tracers. This was reflected in a low maximum uptake value in the liver and elevated blood concentrations. These tracers allow the detection and quantification of impaired hepatobiliary transport.

5. Conclusion

The current study showed that [^{99m}Tc]-DTPA-CDCA as an imaging probe shows better in vitro and in vivo characteristics compared to [^{99m}Tc]-DTPA-CA. It is mainly taken up in the hepatocytes by OATP1B1 andOATP1B3; and is secreted into bile canaliculi via MRP2. Dynamic small-animal SPECT imaging can be a useful noninvasive method of visualizing and quantifying hepatobiliary transporter functionality and disturbances thereof in vivo, which could predict drug pharmacokinetics.

Acknowledgments

The authors would like to thank Kathleen Steemans and Sophie Jonkers (Janssen Pharmaceutical Companies of Johnson & Johnson, Beerse, Belgium), Nico Denecker and Valerie Vandendriessche (Laboratory of Radiopharmacy, Ghent, Belgium) for their help with the in vitro uptake and vesicular efflux assays and Solvo Biotechnologies (Hungary) for the supply of CHO-NTCP and HEK293-OATP1B1 cells.

References

[1] Alrefai WA, Ravinder KG. Bile acid transporters: structure, function, regulation and pathophysiological implications. Pharm Res 2007;24:1803–23.
[2] Kullak-Ublick GA, Stieger B, Hagenbuch B, Meier PJ. Hepatic transport of bile salts. Semin Liver Dis 2000;20:273–92.
[3] Pauli-Magnus C, Stieger B, Meier Y, Kullak-Ublick GA, Meier PJ. Enterohepatic transport of bile salts and genetics of cholestasis. J Hepatol 2005;43:342–57.
[4] Shitara Y, Sato H, Sugiyama Y. Evaluation of drug–drug interaction in the hepatobiliary and renal transport of drugs. Annu Rev Pharmacol Toxicol 2005;45:689–723.
[5] Maddrey WC. Drug-induced hepatotoxicity. J Clin Gastroenterol 2005;39:S83–9.
[6] Padda MS, Sanchez M, Akhtar AJ, Boyer JL. Drug-induced cholestasis. Hepatology 2011;53:1377–87.
[7] Stieger B, Geier A. Genetic variations of bile salt transporters as predisposing factors for drug-induced cholestasis, intrahepatic cholestasis of pregnancy and therapeutic response of viral hepatitis. Expert Opin Drug Metab Toxicol 2011; 7:411–25.
[8] Neyt S, Huisman MT, Vanhove C, De Man H, Vliegen M, Moerman L, et al. *In vivo* visualization and quantification of (disturbed) Oatp mediated hepatic uptake and Mrp2 mediated biliary excretion of [^{99m}Tc]-mebrofenin in mice. J Nucl Med 2013; 54:624–30.
[9] Anelli PL, Lattauda L, Lorusso V, Lox G, Morisetti A, Morosini P, et al. Conjugates of gadolinium complexes to bile acids as hepatocyte-directed contrast agents for magnetic resonance imaging. J Med Chem 2004;47:3629-3641.
[10] Rohacova J, Marin ML, Martinez-Romero A, O'Connor JE, Gomez-Lechon MJ, Donato MT, et al. Synthesis of new, UV-photoactive dansyl derivatives for flow cytometric studies on bile acid uptake. Org Biomol Chem 2009;7:4973–80.
[11] Jia L, Jiang D, Hu P, Li X, Shi H, Cheng D, et al. Synthesis and evaluation of 18F-labeled bile acid compound: a potential PET imaging agent for FXR-related diseases. Nucl Med Biol 2014;41:495–500.
[12] Frisch K, Jakobsen S, Sorenson M, Munk OL, Alstrup AKO, Ott P. [*N*-methyl-11C]cholylsarcosine, a novel bile acid tracer for PET/CT of hepatic excretory function: radiosynthesis and proof-of-concept studies in pigs. J Nucl Med 2012;53:772–8.
[13] Pandey PS, Rai R, Singh RB. Synthesis of cholic acid-based molecular receptors: head-to-head cholaphanes. J Chem Soc 2002;1:918–23.
[14] Sinha D, Shukla S, Chuttani K, Chandra H, Mishra AK. Synthesis and biological evaluation of (99 m)Tc-DTPA-bis(His) as a potential probe for tumor imaging with SPECT. Cancer Biother Radiopharm 2009;24(5):615–20.
[15] Cui Y, König J, Leier I, Buchholz U, Keppler D. Hepatic uptake of bilirubin and its conjugates by the human organic anion transporter SLC21A6. J Biol Chem 2001; 273:9626–30.
[16] Hata S, Wang P, Eftychiou N, Ananthanarayanam M, Batta A, Salen G, et al. Substrate specificities of rat oatp1 and ntcp: implications for hepatic organic anion uptake. Am J Physiol Gastrointest Liver Physiol 2003;285:G829–39.
[17] de Waart DR, Häusler S, Vlaming MLH, Kunne C, Hänggi E, Gruss HJ, et al. Hepatic transport mechanisms of cholyl-L-lysyl-fluorescein. J Pharmacol Exp Ther 2010; 334:78–86.
[18] Milkiewics P, Mills CO, Hubscher SG, Cardenas R, Cardenas T, Williams A, et al. Visualization of the transport of primary and secondary bile acids across liver tissue in rats: *in vivo* study with fluorescent bile acids. J Hepatol 2001;34:4–10.
[19] Baringhaus KH, Matter H, Stengelin S, Kramer W. Substrate specificity of the ileal and the hepatic Na+/bile acid cotransporters of the rabbit. II. A reliable 3D QSAR pharmacophore model for the ileal Na+/bile acid cotransporter. J Lipid Res 1999; 40:2158–68.
[20] Kullak-Ublick GA, Glasa J, Böker C, Oswald M, Grützer U, Hagenbuch B, et al. Chlorambucil-taurocholate is transported by bile acid carriers expressed in human hepatocellular carcinomas. Gastroenterology 1997;113:1295–305.
[21] de Graaf W, Häusler S, Heger M, van Ginhoven TM, van Cappellen G, Benink RJ, et al. Transporters involved in the hepatic uptake of [^{99m}Tc]-mebrofenin and indocyanine green. J Hepatol 2011;54:738–45.
[22] Gerloff T, Stieger B, Hagenbuch B, Madon J, Landmann L, Roth J, et al. The sister of P-glycoprotein represents the canalicular bile salt export pump of mammalian liver. J Biol Chem 1998;273:10046–50.
[23] Carlton VE, Harris BZ, Puffenberger EG, Batta AK, Knisely AS, Robinson DL, et al. Complex inheritance of familial hypercholanemia with associated mutations in TJP2 and BAAT1. Nat Genet 2003;34:91–6.
[24] Kobayashi M, Nakanishi T, Nishi K, Higaki Y, Okudaira H, Ono M, et al. Transport mechanisms of hepatic uptake and bile excretion in clinical hepatobiliary scintigraphy with 99mTc-*N*-pyridoxyl-5-methyltryptophan. Nucl Med Biol 2014;41:338–42.
[25] Dawson PA, Lan T, Rao A. Bile acid transporters. J Lipid Res 2009;50:2340–57.